



Determining Significant Morphological and Hemodynamic Parameters to Assess the Rupture Risk of Cerebral Aneurysms

Nicolás Amigo^{1,2} · Álvaro Valencia¹

Received: 9 July 2017 / Accepted: 30 March 2018 / Published online: 9 April 2018
© Taiwanese Society of Biomedical Engineering 2018

Abstract

Hemodynamics and morphology are recognized as major factors in the rupture risk of cerebral aneurysms, and exploration of their relationship is necessary to establish a method that can be employed by clinicians to assess the likelihood of rupture. In this work, morphological analysis and computational fluid dynamics were carried out to examine a database of 58 lateral cerebral aneurysms (26 ruptured and 32 unruptured) distributed among 49 patients. Eight morphological and six hemodynamic parameters were calculated and evaluated for statistical significance. It was observed that size ratio (SR), systolic wall shear stress (SWSS), diastolic wall shear stress (DWSS) and relative residence time (RRT) were statistically significant. The SR, DWSS, SWSS, and RRT were employed in multivariate logistic regression, obtaining a combined morphological–hemodynamic model, a pure morphological model, and a pure hemodynamic model to evaluate the odds ratio for rupture risk. The combined model had the highest efficiency, but no distinctive difference existed in the predictive capacity of the three models.

Keywords Morphology · Hemodynamic · Cerebral aneurysm · Rupture risk

Abbreviations

CFD	Computational fluid dynamics
WSS	Wall shear stress
AR	Aspect ratio
SR	Size ratio
BNF	Bottleneck factor
NSI	Nonsphericity index
UI	Undulation index
α_A	Aneurysm angle
α_F	Flow angle
α_V	Vessel angle
DWSS	Diastolic wall shear stress
SWSS	Systolic wall shear stress
TAWSS	Time-averaged wall shear stress
RRT	Relative residence time

OSI	Oscillatory shear index
AFI	Aneurysm formation index
ROC	Receiver operating characteristics
AUC	Area under the curve

1 Introduction

It is well known that cerebral aneurysms constitute a risk since their rupture releases blood, causing subarachnoid hemorrhage, morbidity and mortality [1, 2]. Nevertheless, aneurysm treatment is often a complex process for clinicians to carry out, and it can have negative outcomes on patients. Therefore, it is desirable to establish a method for the assessment of rupture risk. Morphological analyses have shown that geometric parameters, such as size, aspect ratio (AR) and aneurysm flow angle, have an association with rupture [3–6]. However, recent computational fluid dynamics (CFD) studies have discussed the role that hemodynamic factors play in the pathogenesis, progression, and rupture of cerebral aneurysms. Wall shear stress (WSS), oscillatory shear index (OSI), and relative residence time (RRT) have been proposed as indicators of aneurysm rupture risk [7–10]. Therefore, it is necessary to develop a combined hemodynamic–morphological approach to further investigate rupture status.

✉ Nicolás Amigo
nico.amigo.a@gmail.com
Álvaro Valencia
alvalenc@ing.uchile.cl

¹ Departamento de Ingeniería Mecánica, Universidad de Chile, Beauchef 851, Santiago, Chile

² Núcleo de Matemáticas, Física y Estadística, Facultad de Ciencias, Universidad Mayor, Manuel Montt 367, Providencia, Santiago, Chile

The aim of this study was to identify significant morphological and hemodynamic parameters that discriminate rupture risk. For this purpose, we performed CFD simulations and morphological characterization of 58 patient-specific lateral cerebral aneurysm models obtained from 49 patients. The aneurysms were located at different cerebral regions: the basilar artery, the internal carotid artery, the middle cerebral artery, the pericallosal artery, the posterior communicating artery and the posterior inferior cerebellar artery. All patient-specific geometries were reconstructed from 3D rotational angiography image data. Eight morphological and six hemodynamic parameters were computed straight from medical images and CFD simulations, respectively. Statistical analysis was carried out to assess the statistical significance of each quantity. This work is organized as follows: Sect. 2 explains the simulation procedure and the tools employed for the analysis, Sect. 3 presents and discusses the results, and finally, Sect. 4 draws conclusions.

2 Materials and Methods

2.1 Computational Method and Boundary Conditions

The patient-specific lateral cerebral aneurysm images were provided by the Instituto de Neurocirugía Asenjo and were obtained with a Philips Integris Allura 3D Rotational Angiograph. A total of 26 ruptured and 32 unruptured aneurysms, distributed among 49 models, were reconstructed for the simulation software Ansys Fluent, following the procedure described by Valencia et al. [11]. Here, we note that the status of all aneurysms was determined during image acquisition and that their evolution was not studied in this work. In addition, from now on, the model corresponding to patient number N is referred to as Case N . The volume mesh was constructed using an unstructured tetrahedral grid with a mesh density of 1500 cells/mm³. The maximum edge size of the cells was set to 0.2 mm. Thus, the system with the maximum number of cells had a volume of 1521 mm³ and 2,265,413 elements, whereas the system with the minimum number of cells had a volume of 218 mm³ and 322,215 elements. As an example, the mesh of a given system is shown in Fig. 1. Higher mesh densities were also studied (2500 and 3500 cells/mm³), but they were not considered in this work since the differences in the mean and maximum WSS during systole were below 3% when compared to the lowest mesh density. Computational fluid dynamic simulations were performed using the PISO scheme. Velocities and pressure were interpolated with a second order upwind and a second order scheme, respectively. Time was discretized using a second order implicit formulation, and

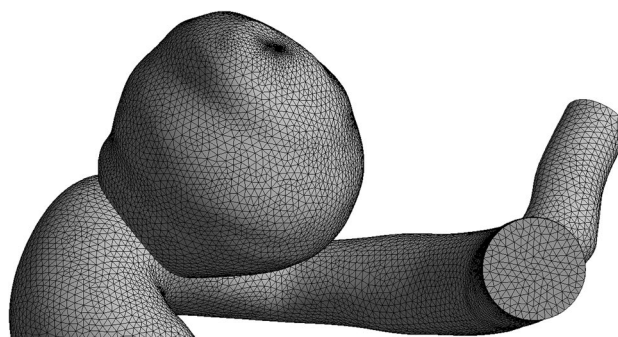


Fig. 1 Tetrahedral mesh for a given patient-specific cerebral aneurysm

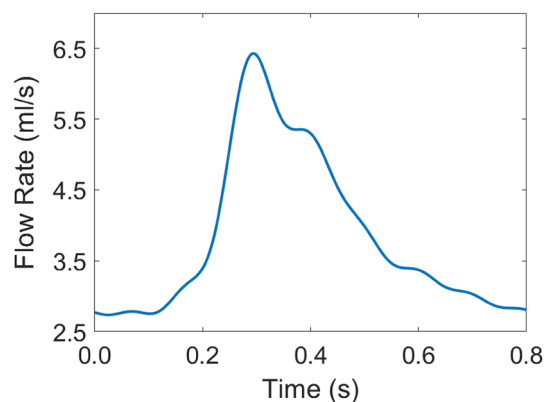


Fig. 2 Example of flow rate used as the inlet condition

the time step was chosen as $\Delta t = 0.0005$ s. Residuals of the momentum and continuity equations were kept below 10^{-3} . Two cardiac cycles of 0.85 s were simulated, and the results were taken from the second cycle. Blood was assumed to be an incompressible Casson fluid [12, 13] with a density of 1065 kg/m³. The flow was modeled as laminar. All simulations were run using double precision on a machine with 16 GB RAM and an Intel i7 CPU with four physical cores.

A Womersley velocity profile was set at the inlet, which was obtained as follows. First, 70 blood pulses of different patients, measured in their internal carotid artery using Doppler ultrasound, were averaged, obtaining $\bar{V}(t)$. Second, the blood flow of each case was calculated as $Q_i(t) = A_i \bar{V}(t)$, where A_i is the inlet area of case i . Lastly, $Q_i(t)$ was fitted to a Fourier series, obtaining the coefficients $Q_i^n(t)$, which were used to calculate the Womersley velocity profile. An example of flow rate is shown in Fig. 2. We remark that the first step allowed us to have the same average inlet velocity in all cases, avoiding an extra variable associated with different inflow conditions as explained by Valencia et al. [14]. No-slip condition was applied to all surfaces, and a pressure pulse oscillating between

80 and 120 mmHg, calculated from a three-element Windkessel circuit, was set to all outlets. This pulse is shown in Fig. 3.

2.2 Morphological Parameters

Eight morphological parameters were defined to characterize each aneurysm: AR, size ratio (SR), bottleneck factor (BNF), nonsphericity index (NSI), undulation index (UI), aneurysm angle (α_A), flow angle (α_F) and vessel angle (α_V). The AR was defined as the ratio of the maximum perpendicular height to the neck diameter, the SR was defined as the ratio of the maximum perpendicular height to the parent vessel diameter, and the BNF was defined as the ratio of the width to the neck. The NSI was calculated as follows:

$$NSI = 1 - (18\pi)^{1/3} \frac{V^{2/3}}{S},$$

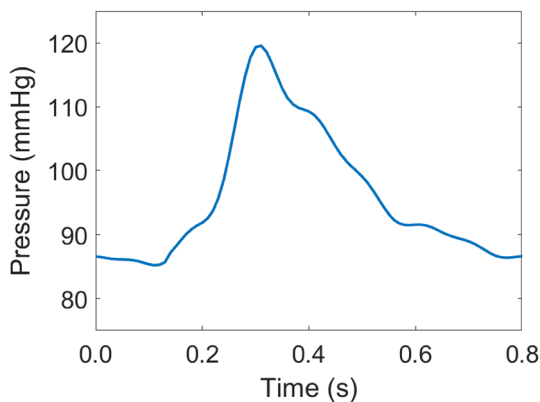
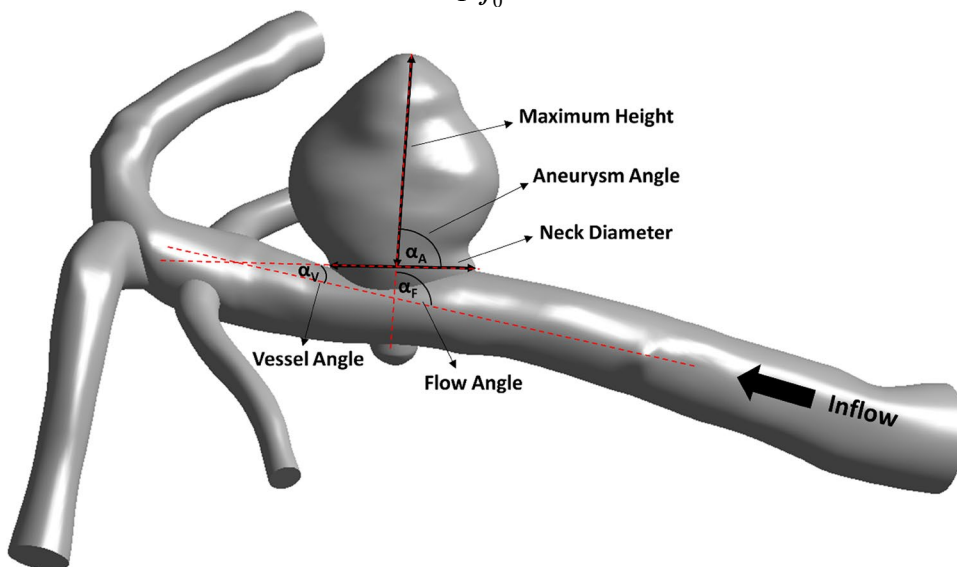


Fig. 3 Pressure waveform employed as the boundary condition for all outlets

Fig. 4 Definition of angles α_A , α_F and α_V



where V is the volume of the aneurysm and S is its surface, whereas UI was obtained as follows:

$$UI = 1 - \frac{V}{V_{ch}},$$

where V_{ch} is the convex hull, which is the smallest volume that fully encloses the aneurysm and that is convex at all points [15]. The α_A was defined as the angle between the neck of the aneurysm and the maximum height of the aneurysm, α_F was defined as the angle between the maximum height of the aneurysm and the parent vessel, and α_V was defined as the angle between the parent vessel and the plane of the aneurysm neck. For more details, these three angles are shown in Fig. 4.

2.3 Hemodynamic Parameters

Six hemodynamic parameters were calculated for each aneurysm: diastolic WSS (DWSS), systolic WSS (SWSS), time-averaged WSS (TAWSS), RRT, OSI, and aneurysm formation index (AFI).

SWSS and DWSS were calculated as the WSS, τ_{ω} , evaluated at the maximum of the systole, t_s , and the minimum of the diastole, t_d , respectively:

$$SWSS = \tau_{\omega}(\vec{x}, t_s),$$

$$DWSS = \tau_{\omega}(\vec{x}, t_d).$$

Both SWSS and DWSS were further averaged over the aneurysm area and then normalized by the SWSS and DWSS of the parent vessel, respectively.

The TAWSS was computed as the average of the WSS during a cardiac cycle T :

$$TAWSS = \frac{1}{T} \int_0^T |\tau_{\omega}(\vec{x}, t)| dt$$

and then, it was averaged over the aneurysm area and normalized by the TAWSS of the parent vessel.

The OSI compares the mean WSS vector with the mean of the magnitude of the same vector. It was calculated as follows [16]:

$$OSI = \frac{1}{2} \left(1 - \frac{\left| \int_0^T \tau_\omega(\vec{x}, t) dt \right|}{\int_0^T |\tau_\omega(\vec{x}, t)| dt} \right)$$

The quantity was also averaged over the aneurysm area.

The RRT is the residence time of particles near the wall, and it was obtained as follows [17, 18]:

$$RRT = \frac{1}{(1 - 2 \times OSI) \times TAWSS}$$

The RRT was further averaged over the aneurysm area and normalized by the RRT of the parent vessel.

The AFI compares the local orientation of the instantaneous WSS with the direction of TAWSS, ignoring its magnitude. It was calculated as follows [19]:

$$AFI = \frac{\tau_\omega(\vec{x}, t) \cdot TAWSS}{|\tau_\omega(\vec{x}, t)| |TAWSS|}$$

and then, it was averaged over the aneurysm area.

2.4 Statistical Analysis

The mean and standard deviation of each parameter was calculated for the unruptured and ruptured groups.

The Jarque–Bera test was employed to determine whether a parameter was normally distributed or not. The

non-parametric Mann–Whitney U test was performed to assess the statistical significance of abnormally distributed data, whereas the Student’s t-test was used for normally distributed data. A P value below 0.005 was considered to be statistically significant. In addition, receiver operating characteristics (ROC) analysis was performed to obtain the optimal threshold of each parameter. The efficiency of each ROC curve was measured by calculating its area under the curve (AUC). All parameters found to be statistically significant were employed in multivariate logistic regression to identify the most relevant quantities. For comparison purposes, all parameters were scaled to span a range from 0 to 10, which means that a unit increase corresponds to 10% of its observed range. Statistics were carried out using Matlab software (MathWorks).

3 Results and Discussion

3.1 Morphological and Hemodynamic Characterization

The mean and standard deviation of each morphological parameter for the unruptured and ruptured group are presented in Table 1. It is observed that all these quantities had higher values for the ruptured group. Nevertheless, NSI and α_A had small differences when comparing both groups. In addition, NSI, UI and α_A were not statistically significant, which contrasts other works [3, 5]. This result may be due to the bigger database of cases considered in those studies. Moreover, our results revealed that only SR was statistically significant. Nevertheless, it is interesting to note that AR, BNF and α_F had P values close to 0.005, which suggests that a bigger database of aneurysms should be analyzed to assess

Table 1 Morphological and hemodynamic parameters for the ruptured and unruptured groups

	Unruptured	Ruptured	Difference (%)	Normally distributed	P
AR	1.460 ± 0.765	1.759 ± 0.561	4.652	No	0.013
SR	1.550 ± 0.860	2.333 ± 1.006	10.084	Yes	0.002
BNF	1.276 ± 0.427	1.718 ± 0.812	7.384	No	0.021
NSI	0.299 ± 0.062	0.301 ± 0.039	0.234	No	0.679
UI	0.107 ± 0.050	0.126 ± 0.077	4.172	No	0.568
α_A	96.188 ± 18.472	100.167 ± 19.289	1.013	Yes	0.427
α_F	101.917 ± 29.576	118.246 ± 22.896	3.709	No	0.020
α_V	14.190 ± 14.583	20.653 ± 17.914	9.275	No	0.075
DWSS	0.653 ± 0.437	0.346 ± 0.159	15.366	No	0.003
SWSS	0.862 ± 0.586	0.461 ± 0.207	15.156	No	0.004
TAWSS	0.712 ± 0.479	0.416 ± 0.257	13.117	No	0.015
RRT	5.394 ± 9.142	7.948 ± 8.925	9.570	No	0.003
OSI	0.009 ± 0.009	0.014 ± 0.011	10.711	No	0.040
AFI	0.984 ± 0.015	0.974 ± 0.020	0.240	No	0.038

the statistical significance of these three quantities. Table 1 also shows the statistical analysis of hemodynamic parameters. It was observed that DWSS, SWSS and TAWSS were higher in the unruptured group than in the ruptured, which is in good agreement with previous works [9, 20, 21]. Furthermore, both DWSS and SWSS of the unruptured group had a ratio closer to one when compared to the same magnitudes of the ruptured group. This finding means that the WSS inside the aneurysm cavity was similar with that of the parent vessel. Nevertheless, this result must be considered cautiously, since there is significant variation in these values. Figure 5 shows the TAWSS fields for some cases of ruptured and unruptured aneurysms. As commented above, it was seen that, overall, the magnitude of WSS was higher for the unruptured group than for the ruptured group. On the other hand, RRT and OSI were higher for the ruptured group than for the unruptured group, which means that particles tend to spend a longer time near the wall and that WSS changes its direction more frequently during a cardiac cycle. Regarding the AFI, a small difference was observed between both groups, making it difficult to infer its incidence in the risk of rupture. Finally, it was observed that DWSS, SWSS and RRT were statistically significant, which is in good agreement with previous results [9, 22]. However, other hemodynamic parameters, such as OSI and TAWSS, should also be statistically significant, as discussed in other works [9, 20]. Nevertheless, a higher number of cases is probably needed [21]. The optimal thresholds of all morphological and hemodynamic parameters were calculated using ROC analysis. The thresholds and AUC are presented in Table 2. On one hand, it was observed that NSI, UI and α_A had the lowest AUC values. These quantities also had the highest P values. On the other hand, SR had the highest AUC value (0.745)

Table 2 Thresholds and AUC for the morphological and hemodynamic parameters

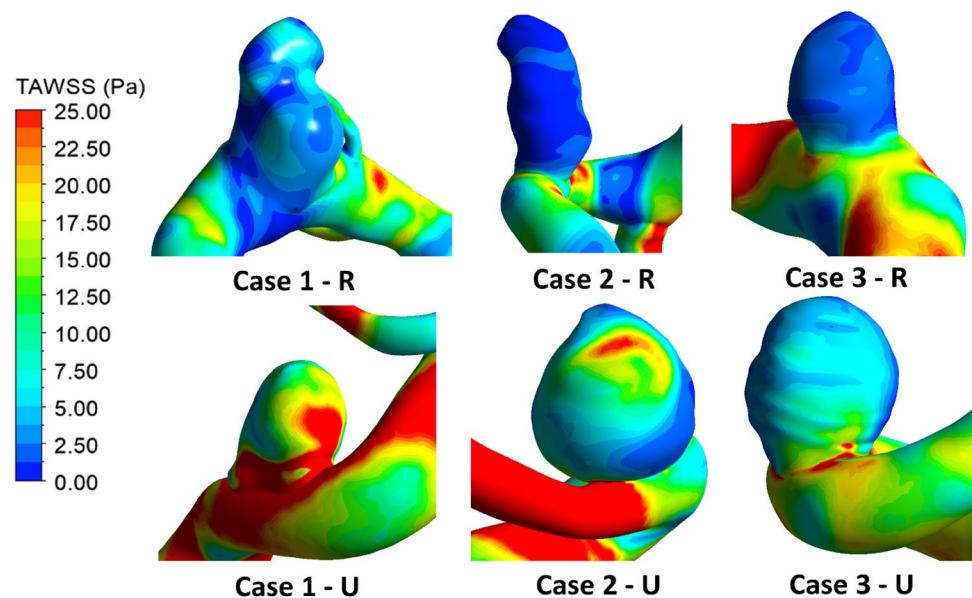
	Threshold	AUC
AR	1.509	0.697
SR	1.617	0.745
BNF	1.277	0.677
NSI	0.321	0.533
UI	0.137	0.545
α_A	94.318	0.402
α_F	116.105	0.679
α_V	12.381	0.637
DWSS	0.662	0.725
SWSS	0.779	0.722
TAWSS	0.608	0.687
RRT	2.525	0.726
OSI	0.007	0.658
AFI	0.986	0.659

and the lowest P value (0.002), which indicates that this parameter is a good indicator for the assessment of rupture risk. This finding is in good agreement with the results of other studies, which reported that SR is a significant predictor, regardless of whether SR is defined on a three-dimensional or two-dimensional basis [9, 22, 23]. The parameter that had the second highest AUC was RRT (~0.726), which was followed by DWSS and SWSS with similar AUC values (0.725 and 0.722, respectively).

3.2 Multivariate Analysis

SR, DWSS, SWSS and RRT were regressed using the stepwise backward elimination process in order to determine a mathematical model for assessment of the risk of rupture

Fig. 5 TAWSS fields for some distinctive cases. R and U stand for ruptured and unruptured, respectively



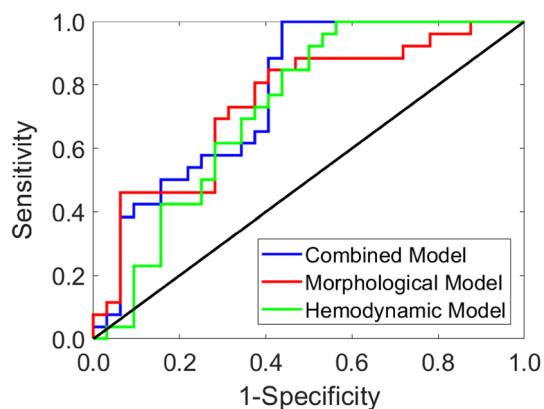


Fig. 6 The ROC curves associated with the combined, pure morphological and pure hemodynamic models

of cerebral aneurysms. Following this procedure, SR and DWSS were retained as relevant parameters. Thus, the odds of rupture was expressed as follows:

$$ODD_{\text{combined}} = e^{0.01+0.33SR-0.59DWSS}$$

The AUC of this model was 0.78. In addition, for a unit increase in SR, the odds of rupture increased 1.39 times, whereas for a unit increase in DWSS, the odds decreased 1.80 times. Hence, the odds of rupture is more sensitive to the DWSS parameter. The efficiency of this model was compared to two other odds: one containing only SR, which we call the pure morphological model, and another containing only DWSS, which we call the pure hemodynamic model. For the first case, the equation was given as follows:

$$ODD_{\text{morph}} = e^{-1.55+0.39SR}$$

The AUC was 0.74 and for a unit increase in SR, the odds increased 1.47 times. For the second case, the model was as follows:

$$ODD_{\text{hemo}} = e^{1.24-0.63DWSS}$$

Here, the AUC was 0.72, whereas for a unit increase in WSS, the odds of rupture decreased 1.89 times. When comparing the three models, the one with the highest efficiency was the odds with both parameters. It is interesting to note that the difference between this model and the pure morphological and pure hemodynamic models was 5.13 and 7.69%, respectively. Thus, the three models had similar efficiencies, and their ROC curves were quite similar (see Fig. 6). Nevertheless, for higher accuracy when predicting the risk of rupture of cerebral aneurysms, the morphological–hemodynamic model should be employed.

It is important to note that the parameters that were statistically significant here partially differ from those obtained in other studies. For example, Xiang et al. [9] indicated that

SR, TAWSS, and OSI were relevant parameters, whereas Qin et al. [24] stated that D/W and EL were the most significant parameters, where D stood for the ratio between the longest dimension from the aneurysm neck to the dome tip, W was the dome width, and EL was the energy loss. Nevertheless, Qin et al. considered only cerebral aneurysms located in the middle cerebral artery, whereas the database of Xiang et al. consisted of aneurysms located in different regions. All in all, the literature available does not provide a sole answer about the most relevant parameters used to assess the risk of rupture of cerebral aneurysms, indicating that more studies are necessary to clarify this subject.

4 Conclusions

Morphological and hemodynamic analyses were performed to determine significant parameters used to assess the risk of rupture of cerebral aneurysms. It was found that SR and DWSS were the most significant parameters. Using both quantities, a combined morphological–hemodynamic model (AUC 0.78), a pure morphological model (AUC 0.74), and a pure hemodynamic model (AUC 0.72) were proposed to evaluate the likelihood of rupture. The combined model had the highest efficiency, but no significant distinction existed between these models. Since SR is relatively simple to calculate from medical images, the pure morphological model can be employed by clinicians to assess the risk of rupture. However, for better accuracy, and considering that CFD simulations are a relatively fast task to carry out, the combined model should be used to predict the likelihood of rupture.

Acknowledgements N. Amigo thanks CONICYT for PhD Fellowship CONICYT-PFCHA/Doctorado Nacional/2015-21151448. The authors would also like to thank Professor Ender Finol and Dr. Sourav Patnaik for their fruitful and constructive suggestions.

References

1. Brisman, J. L., Song, J. K., & Newell, D. W. (2006). Cerebral aneurysms. *The New England Journal of Medicine*, 355(9), 928–939.
2. Wiebers, D. O. (2003). Unruptured intracranial aneurysms: Natural history, clinical outcome, and risks of surgical and endovascular treatment. *The Lancet*, 362(9378), 103–110.
3. Dhar, S., Tremmel, M., Mocco, J., Kim, M., Yamamoto, J., Siddiqui, A. H., et al. (2008). Morphology parameters for intracranial aneurysm rupture risk assessment. *Neurosurgery*, 63(2), 185–197.
4. Baharoglu, M. I., Schirmer, C. M., Hoit, D. A., Gao, B. L., & Malek, A. M. (2010). Aneurysm inflow-angle as a discriminant for rupture in sidewall cerebral aneurysms: Morphometric and computational fluid dynamic analysis. *Stroke*, 41(7), 1423–1430.
5. Lin, N., Ho, A., Charoenvimolphan, N., Frerichs, K. U., Day, A. L., & Du, R. (2013). Analysis of morphological parameters to differentiate rupture status in anterior communicating artery aneurysms. *PLoS ONE*, 8(11), 1–8.

6. Huang, Z. Q., Meng, Z. H., Hou, Z. J., Huang, S. Q., Chen, J. N., Yu, H., et al. (2016). Geometric parameter analysis of ruptured and unruptured aneurysms in patients with symmetric bilateral intracranial aneurysms: A multicenter CT angiography study. *American Journal of Neuroradiology*, *37*(8), 1413–1417.
7. Cebral, J. R., Castro, M. A., Burgess, J. E., Pergolizzi, R. S., Sheridan, M. J., & Putman, C. M. (2005). Characterization of cerebral aneurysms for assessing risk of rupture by using patient-specific computational hemodynamics models. *American Journal of Neuroradiology*, *26*(10), 2550–2559.
8. Valencia, A., Guzmán, A., Finol, E. A., & Amon, C. H. (2006). Blood flow dynamics in saccular aneurysm models of the basilar artery. *Journal of Biomechanical Engineering*, *128*(4), 516–526.
9. Xiang, J., Natarajan, S. K., Tremmel, M., Ma, D., Mocco, J., Hopkins, L. N., et al. (2011). Hemodynamic–morphologic discriminants for intracranial aneurysm rupture. *Stroke*, *42*(1), 144–152.
10. Jing, L., Fan, J., Wang, Y., Li, H., Wang, S., Yang, X., et al. (2015). Morphologic and hemodynamic analysis in the patients with multiple intracranial aneurysms: Ruptured versus unruptured. *PLoS ONE*, *10*(7), 1–12.
11. Valencia, A., Morales, H., Rivera, R., Bravo, E., & Gálvez, M. (2008). Blood flow dynamics in patient-specific cerebral aneurysm models: The relationship between wall shear stress and aneurysm area index through a stenosis. *Medical Engineering and Physics*, *30*(3), 329–340.
12. Papanastasiou, T. C. (1987). Flows of materials with yield. *Journal of Rheology*, *31*, 385–404.
13. Neofytou, P., & Drikakis, D. (2003). Effects of blood models on flows through a stenosis. *The International Journal for Numerical Methods in Fluids*, *43*, 597–635.
14. Valencia, A., Burdiles, P., Ignat, M., Mura, J., Bravo, E., Rivera, R., et al. (2013). Fluid structural analysis of human cerebral aneurysm using their own wall mechanical properties. *Computational and Mathematical Methods in Medicine*, *2013*, 1–18.
15. Raghavan, M. L., Ma, B., & Harbaugh, R. E. (2005). Quantified aneurysm shape and rupture risk. *Journal of Neurosurgery*, *102*(2), 355–362.
16. He, X., & Ku, D. N. (1996). Pulsatile flow in the human left coronary artery bifurcation: Average conditions. *Journal of Biomechanical Engineering*, *118*(1), 74–82.
17. Himburg, H. A., Grzybowski, D. M., Hazel, A. L., LaMack, J. A., Li, X. M., & Friedman, M. H. (2004). Spatial comparison between wall shear stress measures and porcine arterial endothelial permeability. *American Journal of Physiology. Heart and Circulatory Physiology*, *286*, H1916–H1922.
18. Lee, S. W., Antiga, L., & Steinman, D. A. (2009). Correlations among indicators of disturbed flow at the normal carotid bifurcation. *Journal of Biomechanical Engineering*, *131*, 061013.
19. Mantha, A., Karmonik, C., Benndorf, G., Strother, C., & Metcalfe, R. (2006). Hemodynamics in a cerebral artery before and after the formation of an aneurysm. *American Journal of Neuroradiology*, *27*(1), 1113–1118.
20. Miura, Y., Ishida, F., Umeda, Y., Tanemura, H., Suzuki, H., Matsushima, S., et al. (2013). Low wall shear stress is independently associated with the rupture status of middle cerebral artery aneurysms. *Stroke*, *44*(2), 519–521.
21. Xu, J., Yu, Y., Wu, X., Wu, Y., Jiang, C., Wang, S., et al. (2013). Morphological and hemodynamic analysis of mirror posterior communicating artery aneurysms. *PLoS ONE*, *8*(1), 1–7.
22. Xiang, J., Yu, J., Snyder, K. V., Levy, E. I., Siddiqui, A. H., & Meng, H. (2016). Hemodynamic–morphological discriminant models for intracranial aneurysm rupture remain stable with increasing sample size. *Journal of Neurointerventional Surgery*, *8*(1), 104–110.
23. Kashiwazaki, D., Kuroda, S., & Sapporo SAH Study Group. (2013). Size ratio can highly predict rupture risk in intracranial small (< 5 mm) aneurysms. *Stroke*, *44*, 2169–2173.
24. Qin, H., Yang, Q., Zhuang, Q., Long, J., Yang, F., & Zhang, H. (2017). Morphological and hemodynamic parameters for middle cerebral artery bifurcation aneurysm rupture risk assessment. *Journal of Korean Neurosurgical Society*, *60*(5), 504–510.